



MAX-PLANCK-GESELLSCHAFT



Studies in Surface Science and Catalysis Vol. 130, Eds.: A. Corma, F.V. Melo, S. Mendioroz, J.L.G. Fierro, Elsevier, Amsterdam (2000), 2225-2235

Structure-reactivity correlations across the pressure-gap studied on epitaxial iron oxide model catalyst films

C. Kuhrs and W. Weiss

Department of Inorganic Chemistry, Fritz-Haber-Institute of the MPG, Faradayweg 4-6, 14195 Berlin, Germany

Contact: e-mail ranke@fhi-berlin.mpg.de, phone +49 30 8413 3192, fax +49 30 8413 4401

Abstract

Epitaxial model catalyst films of different iron oxide phases and of potassium doped iron oxide were grown onto Pt(111) substrates in order to study the styrene synthesis reaction. The adsorption of ethylbenzene and styrene was investigated by thermal desorption spectroscopy (TDS), and catalytic activities were measured at high gas pressures in a newly designed single-crystal flow reactor. A molecular chemisorption of ethylbenzene and styrene is observed on all three oxide films, where the chemisorption strength of the product molecule styrene decreases if compared to the educt molecule ethylbenzene when going from $\text{Fe}_3\text{O}_4(111)$ over $\alpha\text{-Fe}_2\text{O}_3(0001)$ to $\text{KFe}_x\text{O}_y(111)$. Based on desorption energies and frequency factors determined from the TDS data a Langmuir extrapolation of the adsorbate coverages to the technical styrene synthesis reaction conditions was performed. It suggests an increasing catalytic activity when going from $\text{Fe}_3\text{O}_4(111)$ over $\alpha\text{-Fe}_2\text{O}_3(0001)$ to $\text{KFe}_x\text{O}_y(111)$, because less reactive sites get blocked by the styrene product molecule along this way. This is observed in the high pressure reactivity studies, indicating that the iron oxide surface chemistry does not change significantly across the pressure-gap. We conclude that the product desorption is the rate determining step for this reaction.

1. INTRODUCTION

The technical dehydrogenation of ethylbenzene (EB) to styrene (ST) is carried out over iron oxide based catalysts in excess of steam at temperatures around 900 K. Previous kinetic experiments performed over polycrystalline samples revealed the promoter potassium to increase the catalyst activity by one order of magnitude [1-4], where an active KFeO_2 phase is formed on the catalyst surface under reaction conditions [5,6]. A clear correlation between the catalyst activity and the adsorption-desorption equilibrium constant ratios of the educt and product molecules EB and ST was obtained, where a stronger adsorption of ST leads to a site-blocking effect. In order to study this reaction on an atomic scale we prepare well defined single crystalline model catalyst films of three different iron oxide phases, $\text{Fe}_3\text{O}_4(111)$, $\alpha\text{-Fe}_2\text{O}_3(0001)$ and $\text{KFe}_x\text{O}_y(111)$, by heteroepitaxial growth onto a Pt(111) substrate. The atomic surface structures and stoichiometries of these films were characterized by various techniques including scanning tunneling microscopy (STM), low energy electron diffraction (LEED) and photoelectron spectroscopy [7,8]. They allow us to systematically study correlations between the oxide surface structures, their compositions and catalytic activities. Here we present thermal desorption spectroscopy (TDS) data for the educt and product molecules EB and ST, which reveal information on the kinetics of the elementary steps of adsorption and desorption under ultrahigh vacuum conditions. These TDS experiments were combined with reactivity studies at high gas pressures using a newly designed single crystal flow reactor. An extrapolation of the surface coverages to technical reaction conditions according to the Langmuir model is performed, using desorption energies and frequency factors deduced from the TDS measurements. It is demonstrated that this extrapolation is in line with the activities observed at high gas pressures, indicating that the oxide surface chemistry does not change considerably across the pressure-gap.

2. EXPERIMENTAL

As described in detail previously [9], epitaxial $\text{Fe}_3\text{O}_4(111)$ and $\alpha\text{-Fe}_2\text{O}_3(0001)$ films were grown onto Pt(111) samples by repeated cycles of iron deposition and subsequent oxidation in different oxygen pressures. The potassium promoted $\text{KFe}_x\text{O}_y(111)$ films were prepared by potassium deposition onto an epitaxial $\text{Fe}_3\text{O}_4(111)$ film and subsequent annealing as described in [7]. They form a well ordered hexagonal surface structure with a surface composition close to KFeO_2 . The three different oxide films can easily be distinguished by their LEED patterns [9]. All films are 10-30 nm thick. The TDS measurements were performed in an UHV chamber described elsewhere [10]. EB and ST were adsorbed onto the sample at 100 K with exposures given in Langmuir units ($1 \text{ L} = 1.33 \times 10^{-6} \text{ mbar s}$), the heating rate was always 5 K/s. After each TDS run the films were briefly heated to 870 K in 10^{-6} mbar oxygen in order to remove residual cracking products.

A flow reactor designated to the investigation of heterogeneous catalytic reactions on single crystalline metal oxide model catalysts has been designed. It is located in a high pressure cell that is attached to the UHV analysis chamber, from which it can be completely separated by a gate valve. The high pressure cell is also used for the preparation of the $\alpha\text{-Fe}_2\text{O}_3$ films by a high pressure oxidation. After transfer of the samples into the flow reactor cell, which is located inside the high pressure cell, the latter is vented with nitrogen. A constant He carrier gas flow of 10 and 40 ml/min passes through reservoirs with liquid EB and water held at $T=30^\circ\text{C}$, which provides a molar EB: H_2O ratio of 1:10. This gas mixture enters the reaction

volume (roughly 4 ml) through a capillary of 0.2 mm in diameter. In the reactor the sample is heated by two high power fiber-coupled diode lasers with a total optical output power of 100 W. The product gases were injected from a sample loop with a volume of 250 μ l onto the column of a GC/MS, which provides a high detection sensitivity. All gas lines were heated resistively to prevent condensation of educt and product molecules. For more details see ref. [11].

3. RESULTS AND DISCUSSION

3.1. Thermal desorption studies

Fig. 1 shows TD spectra for increasing amounts of EB adsorbed onto the $\text{Fe}_3\text{O}_4(111)$ multilayer film (upper left). At low exposures a desorption signal labelled γ appears at around 420 K. With increasing exposure it becomes very broad and the maximum shifts to 250 K, until saturation is reached at around 1 L. From about 0.6 L on (this can vary from one film to another), an additional physisorbed EB species β is observed which starts to desorb at 207 K (see insert). Finally, at exposures around 4L a third peak α appears at 158 K. It exhibits a common leading edge for all coverages above 4L and corresponds to the zero order desorption of condensed EB multilayers as shown previously [12]. The TD spectra of ST adsorbed onto $\text{Fe}_3\text{O}_4(111)$ are shown in the lower left of fig. 1. Whereas for EB a very broad chemisorption signal extending from 220 to 420 K is observed, two clearly separated desorption peaks can be seen for ST within this temperature range, which both are attributed to chemisorbed species. At low exposures a species labelled γ_2 appears at around 480 K, indicating a considerably stronger interaction of the styrene molecule with the $\text{Fe}_3\text{O}_4(111)$ surface if compared to EB, which desorbs at 420 K. Then a second species γ_1 appears at 380 K, which shifts to 260 K until saturation is reached at around 1.3 L. From about 1.3 L on a physisorbed species β starts to desorb at 215 K, followed by the final desorption of condensed ST multilayers labelled α at 170 K.

TD spectra for increasing amounts of EB adsorbed onto the $\text{Fe}_2\text{O}_3(0001)$ film are shown in the middle of Fig. 1. At low exposures a small signal labelled γ_2 appears at about 370 K, which gets saturated at very small exposures of 0.1 L. In contrast to EB on $\text{Fe}_3\text{O}_4(111)$, a sharp second signal γ_1 appears at 275 K, which shifts to 260 K with increasing exposure until saturation at about 1 L is reached. We attribute both signals γ_1 and γ_2 to chemisorbed EB species. With further increasing exposure a condensed β signal appears at 209-200 K, followed by desorption of condensed EB multilayers labeled α at 160 K. TD spectra of ST adsorbed onto the $\text{Fe}_2\text{O}_3(0001)$ film are shown below. The γ_2 signal is identical to the one for EB, both with respect to desorption temperature and saturation coverage. The styrene γ_1 signal is also similar to the one of EB. It starts to desorb at 300 K and shifts to 260 K when the saturation exposure of about 1.3 L is reached. Here, the initial γ_1 desorption temperature (300 K) is slightly higher than the one of EB (267 K), but the difference has become smaller than the difference between the chemisorbed γ -EB (420 K) and γ_2 -ST species (480 K) on $\text{Fe}_3\text{O}_4(111)$. With further increasing ST exposure the physisorbed β signal appears at 207 K, followed by the condensed α signal at 170 K.

On the right side of Fig.1 TD spectra for increasing amounts of EB adsorbed onto the potassium doped $\text{KFe}_x\text{O}_y(111)$ film are shown. At low exposures a desorption signal labeled γ with a maximum at about 265 K appears. With increasing exposure it slightly shifts to lower temperatures (260 K) until it saturates at about 1 L. Again, we attribute this signal to desorption of chemisorbed EB species. Then a physisorption signal β appears at 230 K, which shifts to 206 K with increasing exposure. Finally, the condensed EB multilayer signal α evolves at 155 K. The ST spectra shown below look very similar to those of EB. There is no difference in the desorption temperatures and saturation coverages of the chemisorbed γ signals of EB and ST. The physisorbed ST species β start to desorb at 238 K, about 20 K higher than the physisorbed EB β signal, followed by the desorption of condensed ST multilayers α .

To summarize, on all oxide films chemisorbed EB and ST species are observed, which get saturated at exposures around 1 L and desorb molecularly with first order kinetics. A quantitative analysis of the TDS data using the threshold analysis [13] reveals desorption energies ranging from 65 to 118 kJ/mol (see Fig.1) and frequency factors between 10^{12} and 10^{13}s^{-1} for these chemisorbed species. For both EB and ST, the chemisorption strength decreases from $\text{Fe}_3\text{O}_4(111)$ over $\alpha\text{-Fe}_2\text{O}_3(0001)$ to $\text{KFe}_x\text{O}_y(111)$. On Fe_3O_4 ST is considerably stronger bound than EB. This can be caused by the additional C-C π -bond in the vinyl group of the ST molecule, which might be oriented parallel to the iron oxide surface. However, on Fe_2O_3 there is no difference in bonding strength for the chemisorbed EB and ST γ_2 minority species, and a considerably smaller difference is seen for the dominating chemisorbed γ_1 species if compared to Fe_3O_4 . On the potassium doped $\text{KFe}_x\text{O}_y(111)$, which is supposed to be the catalytically most active phase, the bonding energies of chemisorbed styrene and ethylbenzene are identical. The different chemisorption energies on the three oxide surfaces must be related to the different geometric and electronic structures at these surfaces, a topic that is addressed by current spectroscopic investigations.

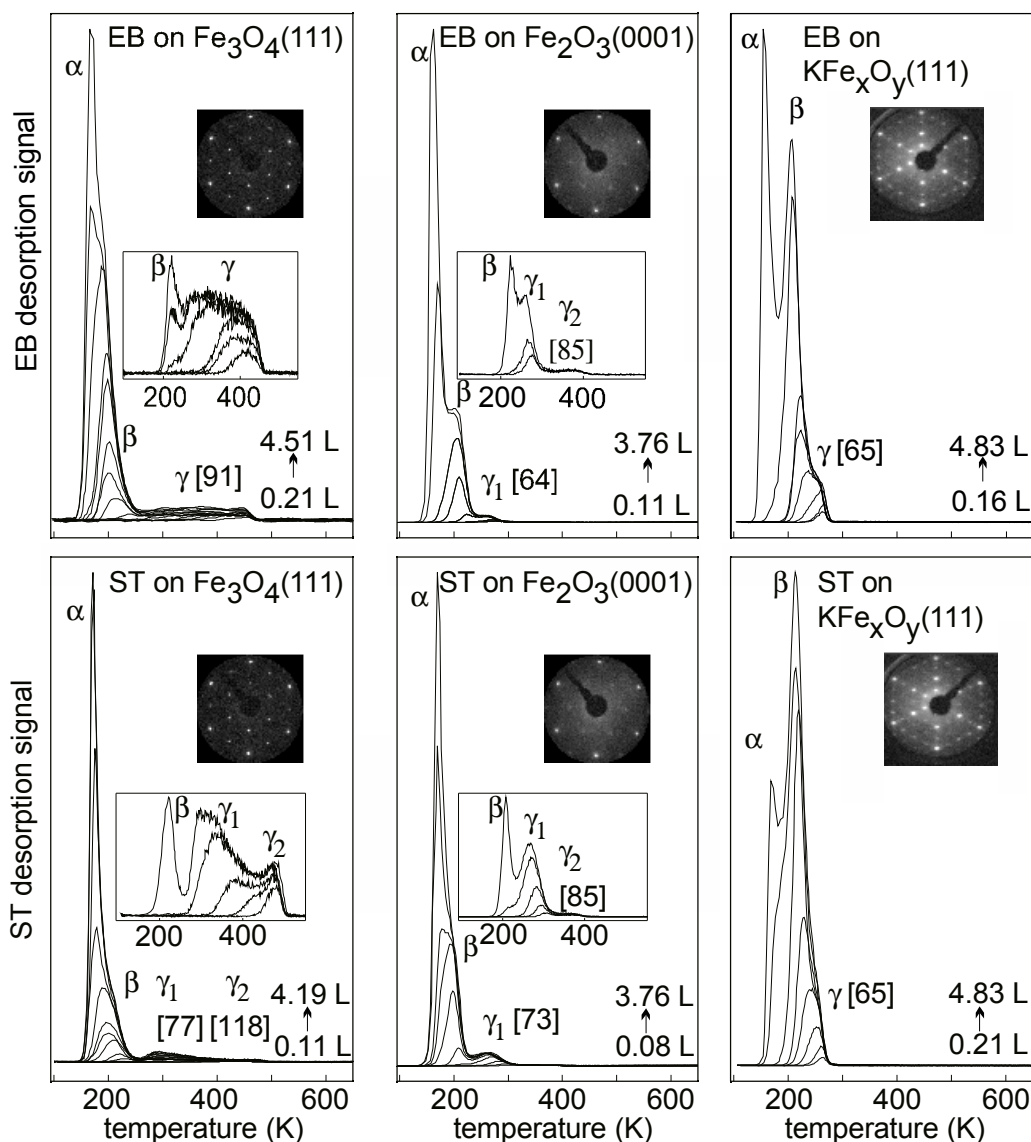


Fig. 1. TD spectra of ethylbenzene (EB) and styrene (ST) adsorbed at $T=100$ K onto $Fe_3O_4(111)$, $\alpha-Fe_2O_3(0001)$ and $KFe_xO_y(111)$. The LEED patterns of the corresponding films taken at $E=60$ eV are also shown. The desorption energies E_{des} for the chemisorbed species are indicated in brackets in kJ/mol.

3.2. Surface coverage extrapolation

An exposure of 1 L of EB or ST at a gas temperature of 300 K corresponds to 1.96×10^{14} molecules cm^{-2} impinging onto the surface. The van-der-Waals area of EB and ST molecules lying flat on the surface is approximately 50 \AA^2 , so that 1 ML defined as a densely packed layer corresponds to $N=2 \times 10^{14}$ molecules cm^{-2} . Since condensation occurs at 150 K for these molecules, a sticking probability near unity is very likely for the adsorption temperature of 100 K. Thus, the saturation exposure of 1L corresponds to about 1 ML (2×10^{14} molecules cm^{-2}), and the chemisorption sites for EB and ST do not represent a minority species as would be expected in case of defect sites. With the Langmuir isotherm we can extrapolate the relative EB and ST surface coverages Θ_i (number of occupied sites divided by the number of available adsorption sites) to the technical styrene synthesis reaction conditions [14]. The Langmuir formalism assumes a single occupation of all surface sites and no mobile precursor adsorption states. Although we observe a precursor adsorption kinetics at $T=100$ K, the lifetime and diffusion length of these precursor species becomes negligible small at $T=900$ K, so that the Langmuir model should describe our systems well. Furthermore, we assume a sticking probability $s_0 \approx 1$ for styrene and ethylbenzene and no activation energies for desorption, $\Delta E_{ad} \approx 0$. As frequency factors usually contain large uncertainties when determined by TDS, we use $\nu_{des} = 10^{13} \text{ s}^{-1}$ for both gases on all surfaces and the desorption energies given in Fig. 1, assuming both quantities to be coverage independent. For simulating the catalyst surface under operation we consider the competitive coadsorption of educt and product molecules EB and ST. Their relative coverages $\Theta_{r,EB}$ and $\Theta_{r,ST}$ can be calculated with the Langmuir isotherm for coadsorption systems, where $\Theta_{r,EB} + \Theta_{r,ST} = \Theta_r$. For equal partial pressures of EB and ST of 100 mbar each, the extrapolation yields on $Fe_3O_4(111)$ $\Theta_r = \Theta_{EB} + \Theta_{ST} = 98\%$ and $\Theta_{EB}/\Theta_{ST} \approx 0.02$, for the majority γ_1 species on $\alpha-Fe_2O_3(0001)$ $\Theta_r = 12\%$ and $\Theta_{EB}/\Theta_{ST} \approx 0.3$, on $KFe_xO_y(111)$ $\Theta_r = 6\%$ and $\Theta_{EB}/\Theta_{ST} \approx 1$. For the catalyst performance the relative occupation of the active chemisorption sites by EB and ST, given by Θ_{EB}/Θ_{ST} , is important. On Fe_3O_4 almost all chemisorption sites are

blocked by the product molecule styrene, on Fe_2O_3 2/3 of the γ_1 (and about half of the γ_2) sites are occupied by styrene, and on the potassium promoted Fe_3O_4 film only half of all chemisorption sites are occupied by styrene. Therefore, the thermodynamic adsorption-desorption parameters determined under ultrahigh vacuum conditions suggest an increasing catalytic activity when going from $\text{Fe}_3\text{O}_4(111)$ over $\text{Fe}_2\text{O}_3(0001)$ to the potassium promoted $\text{KFe}_x\text{O}_y(111)$ film, because the product molecule styrene blocks less dehydrogenation sites along this direction.

3.2. Catalytic activities at high pressures

Reactor experiments with the newly designed single crystal flow reactor were done on the corresponding model catalyst films at a temperature of 600°C. Assuming saturation of the helium carrier gas flows with ethylbenzene and water, 6.7×10^{-6} mol/min of EB and 6.7×10^{-5}

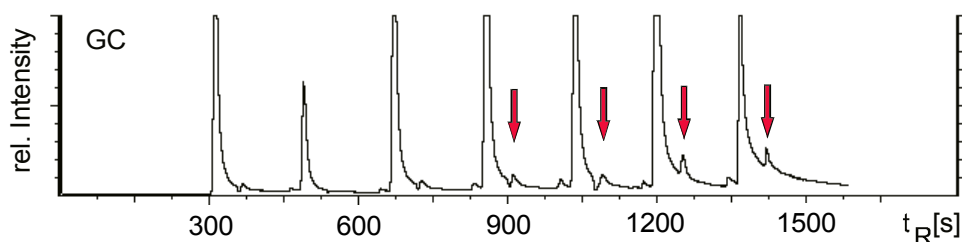


Fig. 2. Reactor experiment on the $\text{KFe}_x\text{O}_y(111)$ film. The arrows indicate the styrene signal in the gas chromatogram, as was confirmed by mass spectrometry.

mol/min of water enter into the reactor. With a reactor volume of about 4 ml and a total gas flow of 50 ml/min a residence time of about 5 s can be estimated. Whereas no conversion to styrene is observed on the $\text{Fe}_3\text{O}_4(111)$ film, conversions of about 1.5% on $\text{Fe}_2\text{O}_3(0001)$ and 3.5% on $\text{KFe}_x\text{O}_y(111)$ (see Fig.2) were observed after some activation periods. These results agree with the suggestions obtained from the extrapolation of the TDS data. In comparison to rates of the technical reaction, the rate observed on the KFe_xO_y film here is about one order of magnitude higher. This probably is due to the fact that in our experiment the flow of educt molecule per catalyst surface area is 10^4 times higher if compared to technical reactors.

4. CONCLUSIONS

The catalytic activity of single crystalline iron oxide and potassium promoted iron oxide model catalyst films increases from $\text{Fe}_3\text{O}_4(111)$ over α - $\text{Fe}_2\text{O}_3(0001)$ to $\text{KFe}_x\text{O}_y(111)$. This is in line with the kinetic adsorption parameters of EB and ST determined by TDS, indicating that the iron oxide surface chemistry does not change significantly across the pressure gap. In accordance with previous kinetic experiments performed on polycrystalline samples, our results suggest that the increasing activity is caused by the easier desorption of the product molecule styrene, that means that the product desorption is the rate determining step. The deprotonation of the C-H groups of the ethyl group of the EB molecule requires the simultaneous action of basic oxygen and neighboring acidic iron sites. Potassium as an electron donor can increase the basicity of the oxygen sites, which increases the catalytic activity. At the same time an electron transfer from the reaction intermediate to an acidic Fe^{3+} site takes place. This might be the reason why Fe_3O_4 is not active, since less Fe^{3+} species exist in this phase when compared to Fe_2O_3 . This was also shown in recent batch reactor experiments performed over the same $\text{Fe}_3\text{O}_4(111)$ and α - $\text{Fe}_2\text{O}_3(0001)$ films [15].

REFERENCES

1. E.H. Lee; Catal. Rev. 8 (1973) 285.
2. T. Hirano; Appl. Catal. 26 (1986) 65, Appl. Catal. 28 (1986) 119.
3. K. Coulter, D.W. Goodman and R.G. More; Catal. Lett. 31 (1995) 1.
4. W.P. Addiego, C.A. Estrada, D.W. Goodman, M.P. Rosynek, R.G. Windham; J. Catal. 146 (1994) 407.
5. M. Muhler, J. Schütze, M. Wesemann, T. Rayment, A. Dent, R. Schlögl, G. Ertl; J. Catal. 126 (1990) 339.
6. M. Muhler, R. Schlögl and G. Ertl; J. of Catal. 138 (1992) 413.
7. Sh. K. Shaikhutdinov, Y. Joseph, C. Kuhrs, W. Ranke and W. Weiss; Farad. Disc. 114 (1999), 363.
8. Th. Schedel-Niedrig, W. Weiss and R. Schlögl; Phys. Rev. B 52 (1995) 17449.
9. W. Weiss; Surf. Sci. 377 (1997) 943.
10. W. Weiss et al., J. Vac. Sci. & Technol. A 16 (1998) 21.
11. C. Kuhrs, M. Swoboda and W. Weiss; submitted to Topics in Catalysis.
12. D. Zscherpel, W. Weiss and R. Schlögl; Surf. Sci., 382 (1997) 326.
13. E. Habenschaden, J. Küppers; Surface Science 138 (1984) L147.
14. K. Christmann; Surface Physical Chemistry, Steinkopff, Darmstadt 1991.
15. W. Weiss, D. Zscherpel, R. Schlögl; Catal. Lett., 52 (1998) 215.